Molecular line search toward the flaring 6.7-GHz methanol masers of G 24.33+0.13 and G 359.62–0.24: rare maser transitions detected

T. P. McCarthy,[1]⋆ G. Orosz,[1] S. P. Ellingsen,[1] S. L. Breen,[2] M. A. Voronkov,[3] R. A. Burns,[4,5]
M. Olech,[6] Y. Yonekura,[7] T. Hirota,[4,8] L. J. Hyland,[1] and P. Wolak[9]

[1] *School of Natural Sciences, University of Tasmania, Private Bag 37, Hobart, Tasmania 7001, Australia*
[2] *SKAO, Jodrell Bank, Lower Withington, Macclesfield, Cheshire, SK11 9FT, UK*
[3] *CSIRO Space & Astronomy, PO Box 76, Epping, NSW 2121, Australia*
[4] *Mizusawa VLBI Observatory, National Astronomical Observatory of Japan, 2-21-1 Osawa, Mitaka, Tokyo 181-8588, Japan*
[5] *Korea Astronomy and Space Science Institute, 776 Daedeokdae-ro, Yuseong-gu, Daejeon 34055, Republic of Korea*
[6] *Space Radio-Diagnostics Research Centre, University of Warmia and Mazury, ul.Oczapowskiego 2, 10-719 Olsztyn, Poland*
[7] *Center for Astronomy, Ibaraki University, 2-1-1 Bunkyo, Mito, Ibaraki 310-8512, Japan*
[8] *Department of Astronomical Sciences, SOKENDAI (The Graduate University for Advanced Studies), Osawa 2-21-1, Mitaka-shi, Tokyo 181-8588*
[9] *Institute of Astronomy, Faculty of Physics, Astronomy and Informatics, Nicolaus Copernicus University, Grudziadzka 5, 87-100 Torun, Poland*

20 October 2021

ABSTRACT

We have performed a molecular line search toward the flaring 6.7-GHz masers G 24.33+0.13 and G 359.62–0.24 using the Australia Telescope Compact Array. We present spectra of the 6.7-GHz class II methanol and 22.2-GHz water masers toward these sources and provide comparison with other recent flaring events these sources have experienced. We also detect the fourth example of a 23.4-GHz class I methanol maser, and the eleventh example of a 4.8-GHz formaldehyde maser toward G 24.33+0.13. Alongside these results, we observe the previously detected ammonia (3,3) emission and report upper limits on the presence of various other cm-wavelength methanol, ammonia and OH transitions. Our results are consistent with the flaring of G 24.33+0.13 being driven by a variable accretion rate in the host high-mass young stellar object.

Key words: masers – radio lines: stars

1 INTRODUCTION

Astronomical maser emission has been detected from a wide array of different transitions from the methanol molecular species (e.g. Barrett et al. 1971; Wilson et al. 1984, 1985; Morimoto et al. 1985; Menten 1991; Breen et al. 2019). These masers have proven useful tools for investigating the evolutionary phases and underlying conditions of star-formation regions within our Galaxy (e.g. Fontani et al. 2010; Ellingsen et al. 2011; Breen et al. 2013; Voronkov et al. 2014; Leurini et al. 2016; McCarthy et al. 2018). Methanol masers are pumped through either collisional or radiative interactions, which divides them into class I and class II respectively (Batrla et al. 1987; Menten 1991; Cragg et al. 1992, 2005; Sobolev et al. 1997; Leurini et al. 2016).

The 6.7-GHz class II transition is useful for the study of high-mass star-formation regions as they are typically highly luminous, and exclusively associated with high-mass

star formation (Breen et al. 2013). The class II masers form close to the young stellar objects (YSOs) where they are radiatively pumped via infrared emission from the proto-stars (Walsh et al. 1998; Cragg et al. 2005). Variability in the class II methanol maser line is relatively common on timescales of months to years (Caswell et al. 1995a; Ellingsen 2007). However, these variations are generally not extreme, with peak intensities remaining similar over their timescales of 20 years (Ellingsen 2007). Goedhart et al. (2004) reported the detection of periodic variability in 7 class II maser sources, along with the first detection of rapid and extreme flux density increase (referred to as flares) from the 6.7-GHz line toward several sources (e.g. G 337.92-0.46, G 345.00-0.22, G 359.61-0.24). Although still a rare phenomenon, over the past two decades several flares have been detected from the 6.7-GHz maser line (e.g. Fujisawa et al. 2015; MacLeod et al. 2018; Sugiyama et al. 2019). The transient nature of these flares makes it difficult to determine the exact mechanisms responsible for the events. There are three commonly suggested explanations of this phenomenon: increase in contin-

⋆ Email: tiegem@utas.edu.au

uum source photons; increases in path length of maser cloud along line of sight or underlying maser pumping conditions improving (Deguchi & Watson 1989; Burns et al. 2020a,b).

A link between protostellar accretion outbursts and maser flares has been made in three class II methanol maser sources to date: S255 NIRS 3 (Moscadelli et al. 2017), NGC 6334I-MM1 (Hunter et al. 2018) and G 358.93–0.03 (Burns et al. 2020b). These events in protostars, where accretion rates burst higher than average, are thought to be necessary for the production of high-mass stars (Meyer et al. 2017). These events result in an enhancement of the radiation field which drives the increased luminosity of the class II lines through induction of more favourable pumping conditions. The maser flare associated with the accretion burst in G 358.93–0.03 is of particular importance, with an extensive maser line survey during the flaring period providing the first astronomical detections of 6 class II methanol maser lines, including the first ever detections of torsionally excited maser lines (Breen et al. 2019; Brogan et al. 2019; Chen et al. 2020).

In this paper we report the results of molecular line searches (between $\sim 6 - 10$ GHz and $\sim 19.9 - 24.2$ GHz) towards two recent 6.7-GHz maser flaring events associated with high-mass star-formation (HMSF) regions G 24.33+0.13 and G 359.62–0.24. Both of these sources have had methanol, water and OH masers previously detected (e.g. Caswell et al. 1995c; Caswell 1998; Szymczak et al. 2005; Breen et al. 2010; Chen et al. 2011). Flaring in the class II masers of G 24.33+0.13 has been previously detected in December 2010 by Wolak et al. (2018), in an event that lasted for approximately 450 days. The flare event in G 24.33+0.13 that we report here was first identified by Wolak et al. (2019) on the 5th of September 2019. Monitoring by Goedhart et al. (2004) over the period from 1999 January to 2003 March detected flaring in a single maser component toward G 359.62–0.24, starting in 2000 January and lasting for ~ 500 days, with the other maser components of this source not varying significantly over this time. The current flaring event in G 359.62–0.24 was first reported by the Ibaraki 6.7-GHz Methanol Maser Monitor (iMet) program on the 13th of July 2020 (Yonekura et al. 2016). Notifications of both flaring events were received as part of the collaboration in the M2O program.[1]

2 OBSERVATIONS

The observations reported in this paper were made using the Australia Telescope Compact Array (ATCA). Observations of G 24.33+0.13 were taken as a part of the C3321 non a-priori assignable (NAPA) project on 2019 November 26/27 and during Director's time on 2021 February 21. The single epoch for G 359.62–0.24 was observed during Director's time on 2020 July 25/26. All epochs of observation using the 4–10 GHz frequency setup used the CFB 1M-0.5k mode of the Compact Array Broadband Backend (CABB; Wilson et al. 2011). This CABB configuration allows for two 2 GHz wide bands (2048×1 MHz channels) and up to 16 1 MHz zoom bands (each consisting of 2048×0.5 kHz channels) in each

wide band. Zoom bands are 'stitched' together in order to achieve appropriate velocity coverage where required. The 19 – 24 GHz frequency setup utilised the CFB 64M-32k CABB mode, which consists of two 2 GHz (32×64 MHz channels) wide bands and up to 16 64 MHz zoom bands (each consisting of 2048×32 kHz channels).

The ATCA was configured in the 1.5C array configuration for the 2019 epoch of G 24.33+0.13 (minimum and maximum baselines of 77 and 1485 m respectively, with ca06 flagged) and 6D configuration for the 2021 epoch (minimum and maximum baselines of 77 and 5878 m respectively). For G 359.62–0.24, the array was in the hybrid H214 configuration (minimum and maximum 82 and 247 m respectively, with ca06 flagged). The synthesised beam sizes achieved for each observation epoch are tabulated in Table 1, alongside the phase centre coordinates and total time on-source.

Flux density and bandpass were calibrated with respect to PKS B1934–638 and PKS B1253–055 respectively for all observation epochs. Unresolved quasar sources for phase calibration were chosen from the ATCA Calibrator Database based on brightness, compactness and proximity to our target sources. TXS 1829–106 was selected for G 24.33+0.13 and TXS 1714–336 for G 359.62–0.24. All epochs utilised the same observing strategy of starting with a 10 minute integration on the bandpass calibrator, interleaving 10 minute target scans with 1 minute and 40 seconds on the relevant phase calibrator and finally finishing with a 10 minute scan on the flux density calibrator.

Both sources were searched for lines using the ATCA C/X band receiver, while K band observations were only made toward G 24.33+0.13. Table 2 contains information on all molecular transitions searched towards G 24.33+0.13 and G 359.62–0.24. Director's time observations of G 359.62–0.24 were made using two different C/X band frequency setups which allowed for the inclusion of some additional C/X lines compared to G 24.33+0.13. Target positions for the 6.7-GHz class II methanol masers were taken from the methanol multibeam (MMB) survey (Caswell et al. 2010; Breen et al. 2015). For G 24.33+0.13, poor uv-coverage of our observations (limited hour angle coverage and equatorial declination of G 24.33+0.13), results in a synthesised beam that is highly elongated in the north-south direction even for the epoch utilising a hybrid array configuration. This results in small uncertainty for the right ascension ($\sim 0.5''$), and comparatively large uncertainty in the declination values ($> 3''$) we report in Table 3. The first epoch (2019 November) of G 24.33+0.13 data was taken approximately 3 months (82 days) after the flaring was first reported toward this source, with our second, follow-up epoch (2021 February) 15 months later. This secondary epoch allows us to investigate the quiescent state of G 24.33+0.13 and determine how the detected lines evolved after the flaring event subsided.

Data were reduced using MIRIAD, following standard techniques for ATCA spectral line observations, with primary, secondary and bandpass calibration utilising the sources outlined above. The MIRIAD uvlin task was used to estimate the intensity of line-free spectral channels on each baseline and consequently subtract any contribution from continuum emission away from the spectral line emission. Phase and amplitude self-calibration were performed (where applicable) on any detected emission from the continuum subtracted data, using the brightest components for each pointing. Spectral

---

[1] The Maser Monitoring Organisation (M2O) is a global cooperative of maser monitoring programs. See MaserMonitoring.org.

Table 1. Details of the observation epochs. Right ascension and declination coordinates represent the adopted target position for our observations. Synthesised beam sizes listed with respect to the 6.7-GHz class II methanol maser transition for the $4 - 10$ GHz setup, and the 22.2-GHz water maser line for the $19 - 24$ GHz setup.

Source	Epoch	Array Config.	R.A. h m s	Dec. $°$ $'$ $''$	Synthesised Beam Size	Total Obs. Length	On-source Time
				$4 - 10$ GHz			
G 24.33+0.13	2019 Nov	1.5C	18 35 08.1	−07 35 03.6	$84.2'' \times 4.0'', 1.5°$	5.5 hrs	174 min
	2021 Feb	6D	18 35 08.1	−07 35 03.6	$79.6'' \times 2.5'', 6.6°$	3 hrs	109 min
G 359.62–0.24	2020 Jul	H214	17 45 39.1	−29 23 30.0	$35.0'' \times 20.7'', 64°$	6 hrs	250 min
				$19 - 24$ GHz			
G 24.33+0.13	2019 Nov	1.5C	18 35 08.1	−07 35 03.6	$63.7'' \times 2.2'', 4.0°$	6.6 hrs	165 min

Table 2. Details of the observed transitions towards G 24.33+0.13 and G 359.62–0.24 along with velocity range and RMS noise of the final spectral line cubes. Detected transitions have their details marked in bold. Multiple spectral resolutions were used when searching for the presence of emission, however, as a reference we provide the RMS noise values for all lines using a spectral resolution of 0.1 km s^{-1} (for the 4–10 GHz setup) or 0.5 km s^{-1} (for the higher frequency setup; denoted by a '†'). Uncertainty in the last digit of the adopted rest frequency is indicated by the value in parentheses. Note that the velocity range of the 7.7-GHz spectral line cube for G 24.33+0.13 does not cover the range where emission is observed from other class II methanol lines in this source. This is due to an error in the CABB frequency setup for these observations. Hyphens represent transitions that were not observed in a particular source.

Molecular Species	Transition	Rest Frequency (GHz)	G 24.33+0.13 Vel. Range (km s^{-1})	RMS Noise (mJy)	G 359.62–0.24 Vel. Range (km s^{-1})	RMS Noise (mJy)
CH$_3$OH	$17_{-2} \to 18_{-3}$ E	6.181146(21)[1]	$40 - 140$	6.7	$-40 - 50$	9.1
	$5_1 \to 6_0$ A$^+$	6.6685192(8)[2]	**$40 - 140$**	**7.5**	**$-40 - 60$**	**9.8**
	$12_4 \to 13_3$ A$^-$	7.682246(50)[3]	$24 - 104$	4.9	$-40 - 50$	5.6
	$12_4 \to 13_3$ A$^+$	7.830848(50)[3]	$50 - 140$	5.3	$-40 - 40$	5.8
	$9_{-1} \to 8_{-2}$ E	9.936202(4)[4]	-	-	$2 - 42$	6.3
	$4_3 \to 5_2$ A$^-$	10.058257(12)[4]	-	-	$4 - 40$	6.0
	$2_1 \to 3_0$ E	19.967396(2)[5]	$0 - 200$	4.3†	-	-
	$11_1 \to 10_2$ A$^+$	20.171089(2)[5]	$0 - 200$	4.5†	-	-
	$10_1 \to 11_2$ A$^+$	20.970658(37)[6]	$0 - 200$	5.5†	-	-
	$12_2 \to 11_1$ A$^-$	21.550342(42)[6]	$0 - 200$	6.4†	-	-
	$9_2 \to 10_1$ A$^+$	23.121024(5)[5]	$0 - 200$	7.0†	-	-
	$10_1 \to 9_2$ A$^-$	23.444776(2)[5]	**$0 - 200$**	**6.4†**	-	-
H$_2$CO	$1_{1,0} \to 1_{1,1}$	4.829657(2)[7]	**$75 - 124$**	**8.7**	$-25 - 55$	11.9
H$_2$O	$6_{1,6} \to 5_{2,3}$	22.2350771(1)[8]	**$0 - 200$**	**8.2†**	-	-
NH$_3$	$6_3 \to 6_3$	19.757538(5)[9]	$0 - 200$	4.2†	-	-
	$7_5 \to 7_5$	20.804830(5)[9]	$0 - 200$	5.4†	-	-
	$10_8 \to 10_8$	20.852527(5)[9]	$0 - 200$	5.4†	-	-
	$11_9 \to 11_9$	21.070739(5)[9]	$0 - 200$	5.8†	-	-
	$6_5 \to 6_5$	22.732429(5)[9]	$0 - 200$	7.2†	-	-
	$9_8 \to 9_8$	23.657471(5)[9]	$0 - 200$	6.2†	-	-
	$3_3 \to 3_3$	23.872453(5)[10]	**$0 - 200$**	**6.1†**	-	-
	$4_4 \to 4_4$	24.1394169(1)[11]	$0 - 200$	5.7†	-	-
OH	$^2\Pi_{1/2}, J = 1/2$	4.765562(3)[12]	-	-	$-34 - 46$	9.5
	$^2\Pi_{3/2}, J = 5/2$	6.030747(5)[13]	$50 - 140$	6.9	$-40 - 50$	9.0
	$^2\Pi_{3/2}, J = 5/2$	6.035092(5)[13]	$40 - 140$	6.8	$-20 - 45$	9.2

Note: [1]Pickett et al. (1998), [2]Müller et al. (2004), [3]Tsunekawa et al. (1995), [4]Breckenridge & Kukolich (1995), [5]Mehrotra et al. (1985), [6]Xu & Lovas (1997),[7]Kukolich (1975), [8]Kukolich (1969), [9]Poynter & Kakar (1975), [10]Kukolich (1967), [11]Kukolich & Wofsy (1970), [12]Radford (1968) and [13]Meerts & Dymanus (1975).

line data from each transition were imaged over the maximum possible velocity range (dependent on constraints of our frequency setup) with various spectral resolutions while searching for evidence of emission. For reference purposes, details of the final spectral line cubes (including 1σ RMS noise values), imaged with a spectral resolution of 0.1 km s^{-1}, can be found in Table 2. The MIRIAD task imfit was used to extract locations and peak flux density values for the detected emission, imfit reports the peak value and location of a two-

dimensional Gaussian fit to a single velocity plane within the continuum subtracted spectral line cube.

3 RESULTS

3.1 G 24.33+0.13

We detected emission from the 6.7-GHz ($5_1 \to 6_0$ A$^+$) and 23.4 ($10_1 \to 9_2$ A$^-$) methanol, 22.2-GHz ($6_1 \to 5_2$) water, 23.9-GHz ($3_3 \to 3_3$) ammonia and 4.8-GHz formaldehyde

Table 3. Details of the detected spectral line emission. Velocity is with respect to local standard of rest. Locations and peak flux density of maser emission were extracted using the imfit MIRIAD task on the brightest component from the spectral line cubes. Positional uncertainties (from fitting) are $\sim 0.5''$, except for declination values for G 24.33+0.13 which are $\sim 3''$.

Target Source	Epoch	Molecular Species	Line	R.A. (J2000) h m s	Dec. (J2000) $^\circ$ $'$ $''$	Flux Density Peak (Jy)	Flux Density Integrated (Jy km s^{-1})	Peak Velocity (km s^{-1})	Velocity Range (km s^{-1})
G 24.33+0.13	2019 Nov	CH$_3$OH	6.7-GHz	18 35 08.1	-07 35 04.5	60.1	21.9	115.3	$107 - 121$
			23.4-GHz	18 35 08.0	-07 34 57.6	1.13	0.93	113.2	$112.8 - 113.6$
		H$_2$CO	4.8-GHz	18 35 08.1	-07 35 05.9	0.62	0.28	109.3	$107 - 117$
		H$_2$O	22.2-GHz	18 35 08.1	-07 35 06.5	28.2	71.3	124.8	$53 - 128$
		NH$_3$	23.9-GHz	18 35 07.8	-07 35 09.8	0.76	0.82	113.5	$112.8 - 114.4$
	2021 Feb	CH$_3$OH	6.7-GHz	18 35 08.1	-07 35 07.0	6.23	5.7	110.2	$107 - 121$
		H$_2$CO	4.8-GHz	18 35 08.1	-07 35 05.3	0.67	0.18	109.6	$108 - 111$
G 359.62$-$0.24	2020 July	CH$_3$OH	6.7-GHz	17 45 39.1	-29 23 30.5	234.2	32.9	19.5	$18 - 25$

$(1_{1,0} \rightarrow 1_{1,1})$ transitions toward G 24.33+0.13. Details of the spectral line emission from these transitions, along with the epoch they were observed in is tabulated in Table 3. The position of the methanol maser emission is consistent with previously reported values from the MMB survey (Breen et al. 2015), to within our astrometric accuracy ($\sim 0.5''$ and $\sim 3''$ in R.A. and declination respectively). A large number of other potential maser transitions were included in observations toward G 24.33+0.13, but none other than the above resulted in clear detections. Details of the final spectral line cubes for all transitions, including the RMS noise values for a $0.1/0.5$ km s^{-1} channel (dependent on frequency setup), are listed in Table 2. It should be noted that during preparation of this manuscript, private communication revealed that the first detection of formaldehyde maser emission in this source was made by the Tianma 65m Radio Telescope on 2019 September 7 by members of the M2O group (Chen et al. in preparation).

The 6.7-GHz methanol emission consists of a series of maser components spread over the velocity range 107–121 km s^{-1}. During the flare, the spectral profile is dominated by two primary peaks at 113.4 and 115.3 km s^{-1}, with several weaker components (factor of ~ 6 lower flux density) distributed across the rest of the velocity range (see Figure 1). Our second epoch of data, (17 months after the flare was detected), reveals that the flux density of these two peaks has decreased by a factor of ~ 20, with the 110 km s^{-1} feature becoming the brightest maser component (see Figure 1). In addition to the two flaring features dimming, we also see a general decrease in flux density across all maser components in the second epoch. Line widths of the maser components are all approximately 0.5 km s^{-1}.

We observe the 22.2-GHz water maser emission to be spread over a broad velocity range, with similar coverage (from $\sim 50 - 130$ km s^{-1}) to the most recent prior observations reported by Cyganowski et al. (2013). We observe a spectral profile dominated by a 2 component red-shifted feature, approximately twice the flux-density of any previously reported 22.2-GHz water maser feature from this source (see top panel of Figure 2). However, the inherent variability of the H$_2$O maser line prevents meaningful comparison between our post-flare observation and those from several years prior to the event.

The position of the peak formaldehyde emission is consistent (to within our astrometric accuracy) between the two epochs, and at approximately the same location within the star-forming region as the class II methanol maser emission. For the 2019 epoch, the formaldehyde emission spectrum consists of a primary component with a full-width at half maximum of ~ 0.2 km s^{-1} at a velocity of 109.3 km s^{-1}, along with what appears to be 3 much weaker features (see Figure 3). The follow-up epoch from 2021 shows a simplification of this spectral profile to a single narrow component at approximately the same flux density (~ 0.6 Jy), redshifted with respect to the 2019 peak by 0.3 km s^{-1} (see Figure 3). Based on the narrow line width seen from these spectral profiles it is likely that this emission is the result of a maser process. This interpretation will be discussed further in Section 4.3.

The spectral profile of the 23.4-GHz methanol transition consists of a single 1.13 Jy component at 113.2 km s^{-1} (see middle panel of Figure 2), with a FWHM of ~ 0.8 km s^{-1} (this FWHM is an upper limit due to the limited spectral resolution of our frequency setup). The emission is located approximately 7 arcseconds north and 2 arcseconds west of the peak 6.7-GHz emission. As mentioned previously, our observing set up is not particularly sensitive to north-south offsets, however, 7 arcseconds is large enough that we are confident this emission is indeed offset from the class II methanol maser emission. The 23.4-GHz methanol transition has only been found toward three other sources within the Milky Way, G 357.97–0.16, G 343.12–0.06 (Voronkov et al. 2011) and G 305.21+0.21 (Voronkov, private communication), where it was determined to be a class I methanol maser.

Similar to the 23.4-GHz methanol, the ammonia (3,3) spectral profile (bottom panel of Figure 2) is made up of a single component at 113.5 km s^{-1}, with a flux density of 0.76 Jy and FWHM of ~ 0.8 km s^{-1} (similarly to the 23.4-GHz emission, this is an upper limit). The position of the peak emission is also offset by approximately 5 arcseconds south-west of the class II methanol emission.

3.2 G 359.62–0.24

Maser emission from the 6.7-GHz methanol ($5_1 \rightarrow 6_0$ A$^+$) transition was detected toward G 359.62–0.24, with details of this emission tabulated alongside the G 24.33+0.13 information in Table 3. Table 2 contains the 0.1 km s^{-1} channel RMS noise values for the spectral line cubes of both the detected
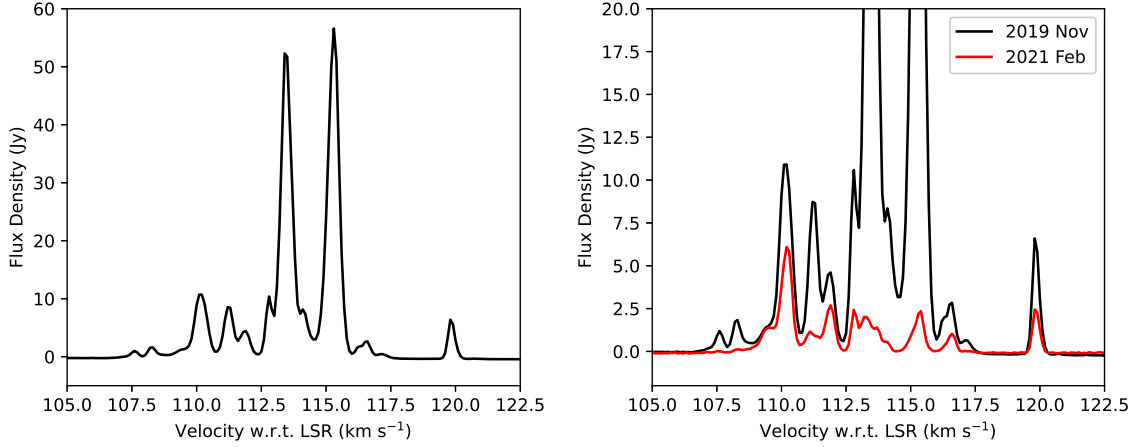
Figure 1. *Left:* Spectrum of 6.7-GHz class II maser emission toward G 24.33+0.13 during the 2019 November flaring epoch. The velocity range has been restricted to the range over which we detect signal. *Right:* A comparison between 6.7-GHz class II maser spectra from our 2019 November and 2021 February epochs.

and non-detected transitions searched for toward G 359.62–0.24.

6.7-GHz class II maser emission is detected over the velocity range $18 - 25$ km s^{-1}, with the primary maser component at 19.5 km s^{-1} (see Figure 4). The maser components have line widths of approximately 0.5 km s^{-1}. This class II emission is at the location of the phase centre for our observations and the reported 6.7-GHz maser position from the MMB survey (Caswell et al. 2010).

4 DISCUSSION

4.1 Comparison with previous class II maser observations toward these sources

4.1.1 G 24.33+0.13

Comparing our flaring 6.7-GHz spectrum to that of the 2010 December flaring event reported by Wolak et al. (2018), we see that the spectral profile is very similar despite the two epochs being almost a decade apart. During this previous flare in G 24.33+0.13, flaring was most prominently seen from the same two features that dominate the spectral profile of our observations (line velocities of 113.4 and 115.3 km s^{-1}), with the flux density of these components increasing by over an order of magnitude compared to quiescent phases (Breen et al. 2015; Yang et al. 2019). Additionally, the peak flux density that the features reach are very similar between the two flaring events. Minor variations are also observed from the other maser components, though notably, the flux density of the 110 and 112 km s^{-1} features appear to be relatively consistent with values reported prior to flaring. We also see the existence of the maser components at line velocities of approximately 108 and 116.5 km s^{-1}, which were only detectable during the peak of the previous flare (Wolak et al. 2018).
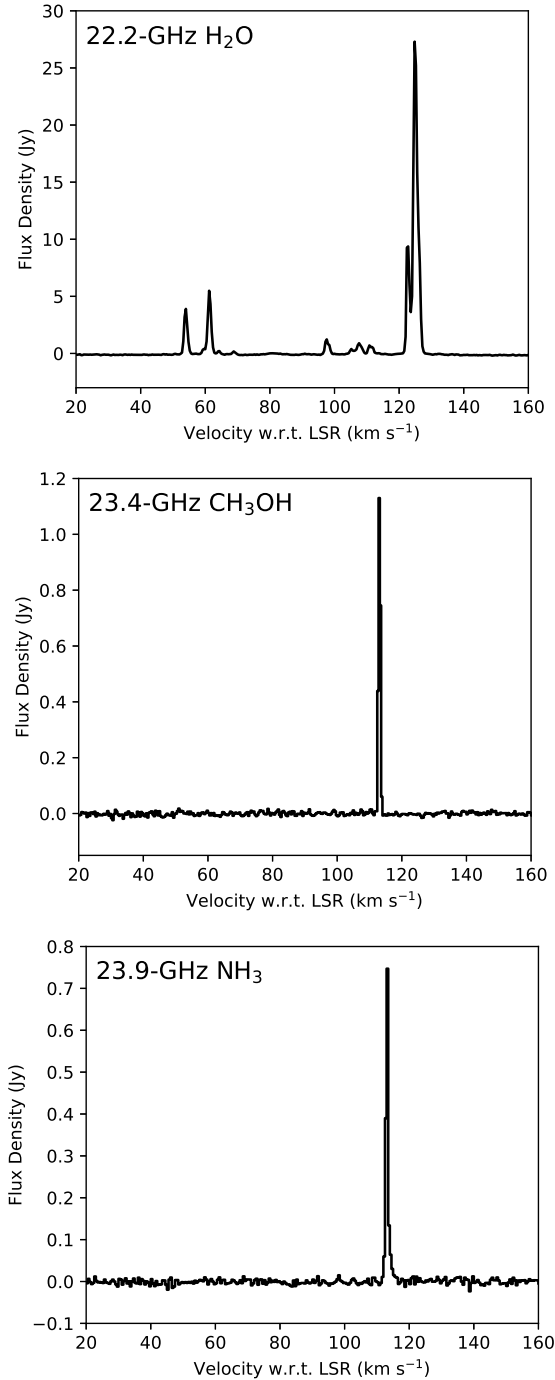
G 24.33+0.13 was observed as part of the MMB survey in 2009 (Breen et al. 2015). The spectral profile of the MMB observations is consistent with that reported by Wolak et al. (2018) before the 2010 flaring event, with the 110 km s^{-1} component significantly brighter (factor of $\sim$

2) than any other emission components. Yang et al. (2019) present Tianma observations of the 6.7-GHz class II methanol emission toward G 24.33+0.13 from 2016 August. Again, the spectral profile is similar to previous quiescent phase observations, however, in this case the relative flux density between the 110 km s^{-1} component and the other maser components is more pronounced (factor of $\sim$ 3 brighter). Comparing our two primary components to those with the same line velocity from Yang et al. (2019) we see an increase in flux density by more than a factor of 25. Comparing the 6.7-GHz class II spectrum from our post flare epoch, we see the methanol emission returning to the same spectral profile that has been previously observed during quiescent phases (Breen et al. 2015; Yang et al. 2019), with the flux density of all features decreasing. Again, the 110 km s^{-1} feature appears to be the least affected by the variability, however, it still shows a flux density decrease of $\sim$ 40% between the 2019 November and 2021 February epochs we report here.
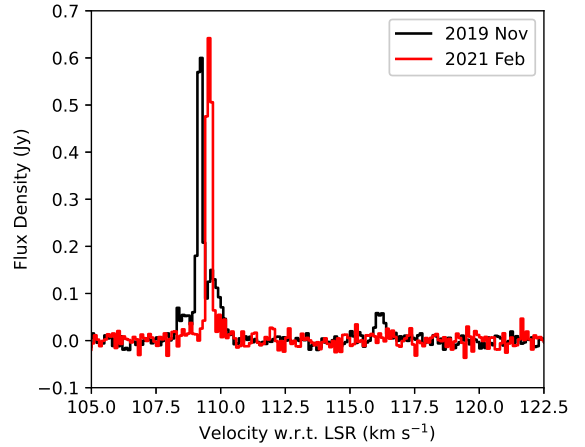
4.1.2 G 359.62–0.24

Variability in G 359.62–0.24 was originally reported by Caswell et al. (1995b) with subsequent long term monitoring of the 6.7-GHz class II emission toward G 359.62–0.24 carried out by Goedhart et al. (2004) over the period from 1999 January to 2003 March. Their monitoring reveals a significant decrease in the flux density of all maser components during this time. In addition to the general decrease in maser flux density during this period, a significant flare ($\sim$ 3 to $\sim$ 11 Jy) from the 18.4 km s^{-1} maser component was observed during 2000 January, lasting approximately 500 days. Even when imaging with the finest spectral resolution possible from our observations ($\sim$ 0.03 km s^{-1}), we can not easily spectrally resolve the 18.4 km s^{-1} component in our observations, however, the spectral profile between 18 and 20 km s^{-1} does appear to consist of 3 or more maser components (see Figure 4). If this is the case, the 18.4 km s^{-1} component would be at approximately the same intensity (11–12 Jy) as seen during the flare reported by Goedhart et al. (2004).

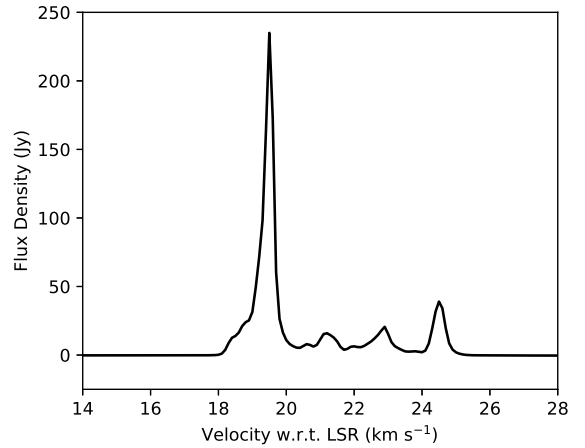The 6.7-GHz emission toward G 359.62–0.24 has been

Figure 2. Spectrum of 22.2-GHz water maser emission (top), 23.4-GHz class I methanol maser emission (middle) and 23.9-GHz class I ammonia maser emission toward G 24.33+0.13 during the 2019 November flaring epoch.

observed as part of the MMB survey (Green et al. 2009; Caswell et al. 2010). Comparison of their spectrum to ours reveals a very similar spectral profile, however we see flux density increases in the 19.5 and 24.5 km s^{-1} components (by a factor of ~ 6 and ~ 2, respectively). The MMB spectrum is from 2008 March, over a decade before the observations we report here, therefore, it is not possible for us to determine exactly what changes in the spectral profile result from the

Figure 3. Comparison of the 4.8-GHz formaldehyde spectra emission toward G 24.33+0.13 from the 2019 November (black) and 2021 February (red) observation epochs.

Figure 4. Spectrum of 6.7-GHz class II maser emission toward G 359.62–0.24.

flare event, and what are due to intrinsic variability of the source. However, the peak flux density of 234 Jy from the 19.5 km s^{-1} component is over a factor of 5 higher than has ever been reported from this source (Goedhart et al. 2004; Caswell et al. 2010), and so it is likely that the flux density of this component has increased during this flare event.

4.2 The fourth detection of 23.4-GHz class I methanol maser emission in the Milky Way

Maser emission in the 23.4-GHz class I methanol maser line has been found toward three other sources to date (G 357.97–0.16, G 343.12–0.06 and G 305.21+0.21; Voronkov et al. 2011, Voronkov private communication). Voronkov et al. (2011) determined this transition to be class I, based on pumping models from Cragg et al. (1992), close positional alignment with other known class I masers and the detection of the line in absorption toward W3(OH) by Menten et al. (1985). Class I methanol masers tend to be offset from the radiatively pumped class II methanol masers (and therefore, the YSOs within the HMSF regions), and associated with shocks

from outflows or cloud-cloud collisions within their host sources (Cyganowski et al. 2009, 2012; Sjouwerman et al. 2010; Voronkov et al. 2014; McCarthy et al. 2018). The off-set we observe between the 23.4-GHz emission and the 6.7-GHz class II maser emission from G 24.33+0.13 is consistent with this expectation, however, as mentioned previously, our array-configuration is not sensitive to north-south offsets and follow-up observations are required to better map the maser components in this source. G 24.33+0.13 is also host to an extended green object (EGO), categorised by Cyganowski et al. (2008) as a region of excess in the *Spitzer* 4.5 μm band that is indicative of outflowing from the YSOs (Cyganowski et al. 2009). A map of this EGO is presented in Figure 10 of Lee et al. (2013), which shows an enhancement of the EGO north-west of the H II region, at the same location from which we detect the 23.4-GHz methanol emission.

The upper limit we place on the FWHM for the 23.4-GHz methanol component (~ 0.8 km s^{-1}) is also a factor of 5 narrower than any thermal emission that has been previously observed toward G 24.33+0.13 (Rathborne et al. 2011). This narrow linewidth, combined with probable association with an outflow and the fact that 23.4-GHz methanol has never been detected as thermal emission indicate that this emission is likely a maser.

4.3 Masing formaldehyde toward G 24.33+0.13

Prior to this work, only ten Galactic H$_2$CO masers had been detected (e.g. Araya et al. 2006; Chen et al. 2017). In this section we will justify our conclusion that the H$_2$CO emission reported here is the result of a maser process.

The spectral profile of the emission in the 2019 November observations seems to consist of 4 narrow emission components, with the FWHM of the primary component being approximately 0.2 km s^{-1}. This narrow line width is consistent with the other known examples of masing formaldehyde (e.g. Araya et al. 2006; Chen et al. 2017). While absorption is commonly observed from the 4.8-GHz formaldehyde transition, thermal emission from the 4.8-GHz H$_2$CO line has only been reported from one source, Orion KL (Zuckerman et al. 1975; Mangum et al. 1993). The reported line width of 3 km s^{-1} for this thermal emission is more than an order of magnitude greater than what we observe toward G 24.33+0.13 (Zuckerman et al. 1975). Additionally, when comparing our two epochs, we see the maser changing from multiple emission components to a single bright component of emission over the 15 month span. Variability like this is not observed from thermal lines, and is a strong argument that the formaldehyde is masing.

The pumping mechanism responsible for population inversion in 4.8-GHz H$_2$CO masers is still poorly understood, with both collisional and radiative origins proposed (Hoffman et al. 2003; Araya et al. 2005, 2006). Correlated variability between H$_2$CO and class II methanol masers has suggested that these masers may share similar radiative excitation mechanisms (Araya et al. 2010), and so far all H$_2$CO masers have been observed towards high-mass star formation regions that also host class II methanol masers. While not always spatially coincident, masers from these two species tend to be distributed over similar distances from the excitation sources (Araya et al. 2010; Chen et al. 2017). Toward G 24.33+0.13, the individual components of the H$_2$CO share

line velocities with the detected 6.7-GHz class II methanol maser components, indicating they are likely distributed over a similar region in this source. However, VLBI observations of the H$_2$CO emission would be required to confirm this.

European VLBI network (EVN) observations of this source by Bartkiewicz et al. (2016), determine a total angular extent of approximately 0.5 arcseconds for the 6.7-GHz class II methanol maser spots. Assuming, as stated above, that the H$_2$CO is distributed over a similar region, this results in a lower limit on the brightness temperature for the peak H$_2$CO emission of more than 10^5 K. As the H$_2$CO is unresolved on our longest baseline (5878 m), we can consider a more conservative angular scale of $2''$ for which we calculate a brightness temperature larger than 10^4 K. Even the conservative estimate of the brightness temperature implies that this emission is the result of a maser process.

Our two epochs do not allow us to determine whether this masing formaldehyde showed evidence of flaring alongside the class II methanol maser emission. The integrated flux density decreases by $\sim 35\%$ in the 15 months between our observations, which is far less dramatic than the $\sim 75\%$ seen from the methanol. Chen et al. (in preparation) will report monitoring of this 4.8-GHz maser with higher temporal resolution across the class II methanol maser flare period in a future publication.

4.4 Ammonia (3,3) emission toward G 24.33+0.13

The metastable ($J = K$) ammonia (3,3) inversion transition has been readily observed as thermal emission (e.g. Wienen et al. 2012; Cyganowski et al. 2013) and much more rarely (8 sources total) as maser emission towards star-formation regions in the Milky Way (Mangum & Wootten 1994; Kraemer & Jackson 1995; Zhang & Ho 1995; Zhang et al. 1999; Hunter et al. 2008; Brogan et al. 2011; Urquhart et al. 2011; Walsh et al. 2011). Masers from metastable ammonia transitions rely on collisional pumping in order to achieve population inversion. Cyganowski et al. (2013) reported emission from the (1,1), (2,2) and (3,3) ammonia transitions toward G 24.33+0.13, with an LSR velocity of 113.7 km s^{-1}. Our interferometric observations detect the (3,3) line at approximately the same LSR velocity, though our peak flux-density is $\sim 30\%$ lower and the upper-limit linewidth for the component is much narrower than the previously observed (3,3) emission. While this narrower linewidth and offset location hint at a potential maser origin, analysis of the emission from each baseline reveals a clear relationship between the spectral profile and baseline length, with our shortest baseline (77 metres) spectrum being comparable in both linewidth and flux-density to that reported by Cyganowski et al. (2013), and the emission completely resolved out on our 1000+ metre baselines. This relationship may be the result of the ammonia (3,3) emission consisting of both a compact (narrow linewidth) and extended (broad linewidth) component, however, further modelling and observations would be required to conclusively determine this.

4.5 Flare mechanisms and comparison to the accretion burst in G 358.93–0.03

The recent accretion burst related 6.7-GHz class II methanol flare in G 358.93–0.03 was accompanied by dramatic flaring in various other class II methanol maser transitions, several of which had never been detected toward an astronomical source previously (e.g. Breen et al. 2019). Similar flaring of rare maser lines (methanol and OH) has also been observed alongside the accretion burst in NGC 6334I (MacLeod et al. 2018). We included a handful of these class II methanol lines in our observations (see Table 2), however, did not see emission from them toward either flaring source. Based on the investigation of the G 358.93–0.03 flare event, emission from these rare methanol transitions (6.2-, 7.7- and 7.8-GHz) had a decay half-life of approximately 10 days (Chen et al. 2020). Assuming similar relative flux density values between the 6.7-GHz and these rare transitions as seen toward G 358.93–0.03 (Breen et al. 2019), we would have been able to easily detect emission from these lines ($> 50\sigma$ detections) toward both these sources if it were present.

While we did not detect any of these additional class II methanol maser transitions, we did observe rare collisionally and radiatively pumped masers toward G 24.33+0.13. The lack of any contemporaneous flaring of other maser lines toward G 359.62–0.24 may suggest a different mechanism (rather than a large accretion burst event) may be driving the flaring in this source. However, due to the small sample of maser flares where such an extensive molecular line search has been conducted, this behaviour (flaring observed from a plethora of transitions) may not be representative of a typical accretion-burst flare and our single observation epoch toward G 359.62–0.24 is not sufficient for us to properly determine the mechanism behind the flaring.

For G 24.33+0.13, the decrease in the flux density of all maser components (see Figure 1) from our second epoch suggests that the flaring does not result from an increase in the maser path length, where we would expect to see variation in a small number of velocity-coherent maser features (e.g. Burns et al. 2020b). The similarity between this flare and that observed in 2010 by Wolak et al. (2018) indicates some long-term periodic mechanism may be responsible for flaring in this source. There have been several periodic 6.7-GHz class II methanol maser sources where the class II methanol maser flux density is correlated with periodic variation in the infrared emission (Stecklum et al. 2018; Olech et al. 2019). In these cases, the infrared radiation field has been identified as scaling with periodic enhancements of the accretion rates in the high-mass YSO, driven by binary interaction. The flaring of G 24.33+0.13 may be driven by a similar interaction, however, the ~ 9 year gap between the two reported flare events is a much larger than the 53 to 540 day periods seen toward other periodic class II methanol maser sources (Olech et al. 2019).

Both G 24.33+0.13 and G 359.62–0.24 have been targets for the iMet maser monitoring program (Yonekura et al. 2016), which has monitored the 6.7-GHz class II maser emission since 2013. An upcoming publication from this program will produce flare profiles for both of these sources (Yonekura et al. in preparation), allowing for comparison against infrared light curves and further investigation of the flare mechanisms.

5 CONCLUSIONS

We present the results of an ATCA molecular line search toward two flaring class II methanol maser sources G 24.33+0.13 and G 359.6-0.24.

Toward G 24.33+0.13 we observe a factor of 25 increase in the flux density of flaring 6.7-GHz class II methanol maser components compared with pre- and post-flare observations. A comparison of the 6.7-GHz spectral profile with the previously observed flare from 2010, reported by Wolak et al. (2018), reveals the same maser components are flaring in both events. Our quiescent phase epoch (15 months later) reveals an across the board decrease in the flux density of the 6.7-GHz class II methanol masers.

We detect 4.8-GHz formaldehyde emission toward G 24.33+0.13. The line-width, estimated brightness temperature, similarity with the class II methanol maser emission and variability in the spectral profile between epochs all indicate that this emission is the result of maser processes. This is the eleventh example of a formaldehyde maser within our Galaxy. Additionally, we report the detection of the fourth example of a 23.4-GHz class I methanol maser, and detection of ammonia (3,3) emission along with presenting a spectrum of the 22.2-GHz water maser emission shortly after the flare event.

Our observations of G 359.6-0.24 show no evidence of any contemporaneous flaring of other methanol (or other species) maser transitions. While this is not conclusive, it is inconsistent with other known examples of accretion burst flares, suggesting that the flaring from this source may instead be caused by another mechanism.

DATA AVAILABILITY

The data underlying this article will be shared on reasonable request to the corresponding author. Australia Telescope Compact Array data is open access 18 months after the date of observation and can be accessed using the Australia Telescope Online Archive (https://atoa.atnf.csiro.au).

REFERENCES

Araya E., Hofner P., Kurtz S., Linz H., Olmi L., Sewilo M., Watson C., Churchwell E., 2005, ApJ, 618, 339

Araya E., Hofner P., Goss W. M., Kurtz S., Linz H., Olmi L., 2006, ApJ, 643, L33

Araya E. D., Hofner P., Goss W. M., Kurtz S., Richards A. M. S., Linz H., Olmi L., Sewiło M., 2010, ApJ, 717, L133

Astropy Collaboration et al., 2013, A&A, 558, A33

Barrett A. H., Schwartz P. R., Waters J. W., 1971, ApJ, 168, L101

Bartkiewicz A., Szymczak M., van Langevelde H. J., 2016, A&A, 587, A104

Batrla W., Matthews H. E., Menten K. M., Walmsley C. M., 1987, Nature, 326, 49

Breckenridge S. M., Kukolich S. G., 1995, ApJ, 438, 504

Breen S. L., Caswell J. L., Ellingsen S. P., Phillips C. J., 2010, MNRAS, 406, 1487

Breen S. L., Ellingsen S. P., Contreras Y., Green J. A., Caswell J. L., Stevens J. B., Dawson J. R., Voronkov M. A., 2013, MNRAS, 435, 524

Breen S. L., et al., 2015, MNRAS, 450, 4109

Breen S. L., Sobolev A. M., Kaczmarek J. F., Ellingsen S. P., McCarthy T. P., Voronkov M. A., 2019, ApJ, 876, L25

Brogan C. L., Hunter T. R., Cyganowski C. J., Friesen R. K., Chandler C. J., Indebetouw R., 2011, ApJ, 739, L16

Brogan C. L., et al., 2019, ApJ, 881, L39

Burns R. A., et al., 2020a, Nature Astronomy, 4, 506

Burns R. A., et al., 2020b, MNRAS, 491, 4069

Caswell J. L., 1998, MNRAS, 297, 215

Caswell J. L., Vaile R. A., Ellingsen S. P., 1995a, Publ. Astron. Soc. Australia, 12, 37

Caswell J. L., Vaile R. A., Ellingsen S. P., Whiteoak J. B., Norris R. P., 1995b, MNRAS, 272, 96

Caswell J. L., Vaile R. A., Forster J. R., 1995c, MNRAS, 277, 210

Caswell J. L., et al., 2010, MNRAS, 404, 1029

Chen X., Ellingsen S. P., Shen Z.-Q., Titmarsh A., Gan C.-G., 2011, ApJS, 196, 9

Chen X., Shen Z.-Q., Ellingsen S. P., Li X.-Q., Yang K., Chen H.-Y., Dong J., 2017, ApJ, 851, L3

Chen X., et al., 2020, ApJ, 890, L22

Cragg D. M., Johns K. P., Godfrey P. D., Brown R. D., 1992, MNRAS, 259, 203

Cragg D. M., Sobolev A. M., Godfrey P. D., 2005, MNRAS, 360, 533

Cyganowski C. J., et al., 2008, AJ, 136, 2391

Cyganowski C. J., Brogan C. L., Hunter T. R., Churchwell E., 2009, ApJ, 702, 1615

Cyganowski C. J., Brogan C. L., Hunter T. R., Zhang Q., Friesen R. K., Indebetouw R., Chandler C. J., 2012, preprint, (arXiv:1210.3366)

Cyganowski C. J., Koda J., Rosolowsky E., Towers S., Donovan Meyer J., Egusa F., Momose R., Robitaille T. P., 2013, ApJ, 764, 61

Deguchi S., Watson W. D., 1989, ApJ, 340, L17

Ellingsen S. P., 2007, MNRAS, 377, 571

Ellingsen S. P., Breen S. L., Sobolev A. M., Voronkov M. A., Caswell J. L., Lo N., 2011, ApJ, 742, 109

Fontani F., Cesaroni R., Furuya R. S., 2010, A&A, 517, A56

Fujisawa K., Yonekura Y., Sugiyama K., Horiuchi H., Hayashi T., Hachisuka K., Matsumoto N., Niinuma K., 2015, The Astronomer's Telegram, 8286, 1

Goedhart S., Gaylard M. J., van der Walt D. J., 2004, MNRAS, 355, 553

Green J. A., et al., 2009, MNRAS, 392, 783

Hoffman I. M., Goss W. M., Palmer P., Richards A. M. S., 2003, ApJ, 598, 1061

Hunter T. R., Brogan C. L., Indebetouw R., Cyganowski C. J., 2008, ApJ, 680, 1271

Hunter T. R., et al., 2018, ApJ, 854, 170

Kraemer K. E., Jackson J. M., 1995, ApJ, 439, L9

Kukolich S. G., 1967, Physical Review, 156, 83

Kukolich S. G., 1969, J. Chem. Phys., 50, 3751

Kukolich S. G., 1975, Journal of the American Chemical Society, 97, 5704

Kukolich S. G., Wofsy S. C., 1970, The Journal of Chemical Physics, 52, 5477

Lee H.-T., et al., 2013, ApJS, 208, 23

Leurini S., Menten K. M., Walmsley C. M., 2016, A&A, 592, A31

MacLeod G. C., et al., 2018, MNRAS, 478, 1077

Mangum J. G., Wootten A., 1994, ApJ, 428, L33

Mangum J. G., Wootten A., Plambeck R. L., 1993, ApJ, 409, 282

McCarthy T. P., Ellingsen S. P., Voronkov M. A., Cimò G., 2018, MNRAS, 477, 507

Meerts W. L., Dymanus A., 1975, Canadian Journal of Physics, 53, 2123

Mehrotra S. C., Dreizler H., Mäder H., 1985, Zeitschrift Naturforschung Teil A, 40, 683

Menten K. M., 1991, ApJ, 380, L75

Menten K. M., Johnston K. J., Wilson T. L., Walmsley C. M., Mauersberger R., Henkel C., 1985, ApJ, 293, L83

Meyer D. M. A., Vorobyov E. I., Kuiper R., Kley W., 2017, MNRAS, 464, L90

Morimoto M., Ohishi M., Kanzawa T., 1985, ApJ, 288, L11

Moscadelli L., et al., 2017, A&A, 600, L8

Müller H. S. P., Menten K. M., Mäder H., 2004, A&A, 428, 1019

Olech M., Szymczak M., Wolak P., Sarniak R., Bartkiewicz A., 2019, MNRAS, 486, 1236

Pickett H. M., Poynter R. L., Cohen E. A., Delitsky M. L., Pearson J. C., Müller H. S. P., 1998, J. Quant. Spectrosc. Radiative Transfer, 60, 883

Poynter R. L., Kakar R. K., 1975, ApJS, 29, 87

Radford H. E., 1968, Review of Scientific Instruments, 39, 1687

Rathborne J. M., Garay G., Jackson J. M., Longmore S., Zhang Q., Simon R., 2011, ApJ, 741, 120

Sjouwerman L. O., Murray C. E., Pihlström Y. M., Fish V. L., Araya E. D., 2010, ApJ, 724, L158

Sobolev A. M., Cragg D. M., Godfrey P. D., 1997, A&A, 324, 211

Stecklum B., Caratti o Garatti A., Hodapp K., Linz H., Moscadelli L., Sanna A., 2018, in Tarchi A., Reid M. J., Castangia P., eds, Vol. 336, Astrophysical Masers: Unlocking the Mysteries of the Universe. pp 37–40 (arXiv:1711.01489), doi:10.1017/S1743921317010511

Sugiyama K., Saito Y., Yonekura Y., Momose M., 2019, The Astronomer's Telegram, 12446, 1

Szymczak M., Pillai T., Menten K. M., 2005, A&A, 434, 613

Tsunekawa S., Ukai T., Toyama A., Takagi K., 1995, Department of Physics, Toyama Univerity, Japan

Urquhart J. S., et al., 2011, MNRAS, 418, 1689

Voronkov M. A., Walsh A. J., Caswell J. L., Ellingsen S. P., Breen S. L., Longmore S. N., Purcell C. R., Urquhart J. S., 2011, MNRAS, 413, 2339

Voronkov M. A., Caswell J. L., Ellingsen S. P., Green J. A., Breen S. L., 2014, MNRAS, 439, 2584

Walsh A. J., Burton M. G., Hyland A. R., Robinson G., 1998, MNRAS, 301, 640

Walsh A. J., et al., 2011, MNRAS, 416, 1764

Wienen M., Wyrowski F., Schuller F., Menten K. M., Walmsley C. M., Bronfman L., Motte F., 2012, A&A, 544, A146

Wilson T. L., Walmsley C. M., Snyder L. E., Jewell P. R., 1984, A&A, 134, L7

Wilson T. L., Walmsley C. M., Menten K. M., Hermsen W., 1985, A&A, 147, L19

Wilson W. E., et al., 2011, MNRAS, 416, 832

Wolak P., Szymczak M., Olech M., Bartkiewicz A., 2018, in Tarchi A., Reid M. J., Castangia P., eds, Vol. 336, Astrophysical

Masers: Unlocking the Mysteries of the Universe. pp 319–320, doi:10.1017/S1743921317009930

Wolak P., Olech M., Szymczak M., Bartkiewicz A., Durjasz M., 2019, The Astronomer's Telegram, 13080, 1

Xu L.-H., Lovas F. J., 1997, Journal of Physical and Chemical Reference Data, 26, 17

Yang K., et al., 2019, ApJS, 241, 18

Yonekura Y., et al., 2016, PASJ, 68, 74

Zhang Q., Ho P. T. P., 1995, ApJ, 450, L63

Zhang Q., Hunter T. R., Sridharan T. K., Cesaroni R., 1999, ApJ, 527, L117

Zuckerman B., Palmer P., Rickard L. J., 1975, ApJ, 197, 571